Supplementary Information

Table of figures

Mass spectra

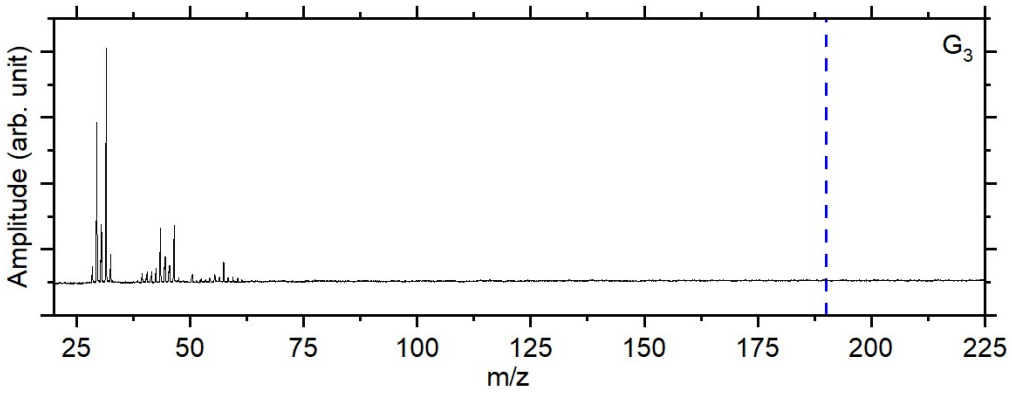

Figure S1: Photodissociation mass spectrum over the full mass range of G_3 measured at 401.6 eV (BESSY II). Here, the mass window was set to see the fragment from m/z 25 to m/z 70. The dashed blue line represents the position of the precursor ion.

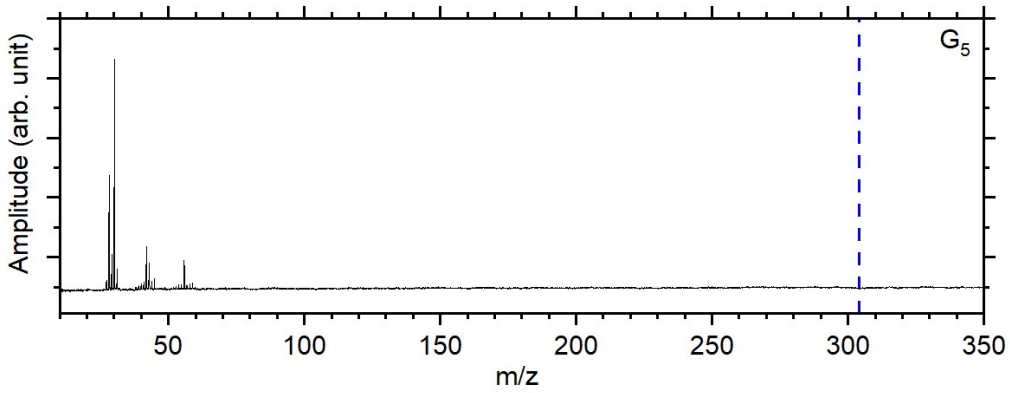

Figure S2: Photodissociation mass spectrum over the full mass range of G_5 measured at 401.6 eV (BESSY II). Here, the mass window was set to see the fragments from m/z 25 to m/z 70. The dashed blue line represents the position of the precursor ion.

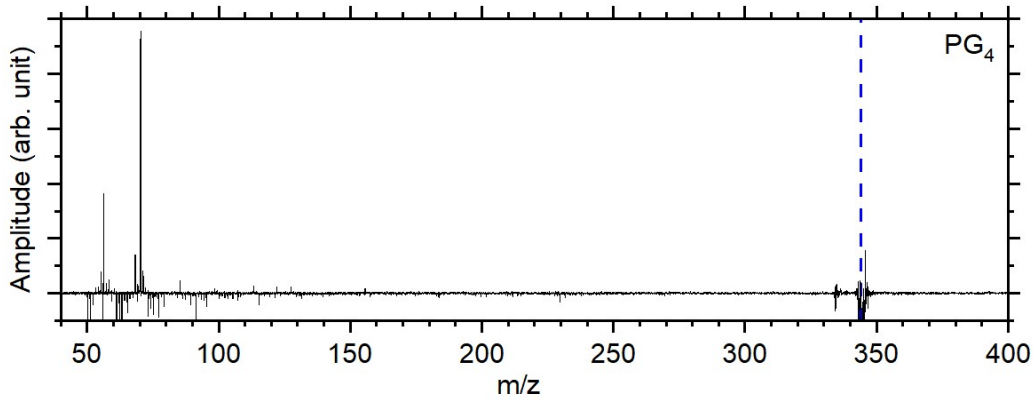

Figure S3: Subtracted photodissociation mass spectrum over the full mass range of PG_4 measured at 401.6 eV (PETRA III). The negative peaks come from the background subtraction. The dashed blue line represents the position of the precursor ion.

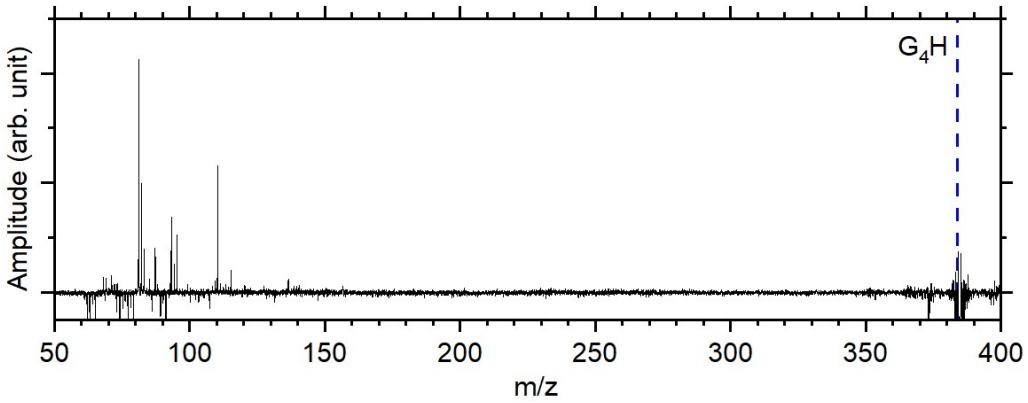

Figure S4: Subtracted photodissociation mass spectrum over the full mass range of G_4H measured at 401.6 eV (PETRA III). The negative peaks come from the background subtraction. The dashed blue line represents the position of the precursor ion.

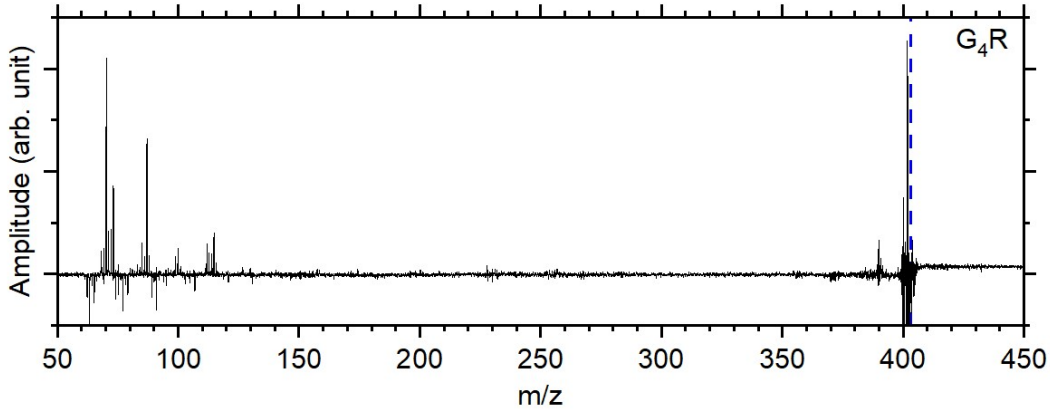

Figure S5: Subtracted photodissociation mass spectrum over the full mass range of G_4R measured at 401.6 eV (PETRA III). The negative peaks come from the background subtraction. The dashed blue line represents the position of the precursor ion.

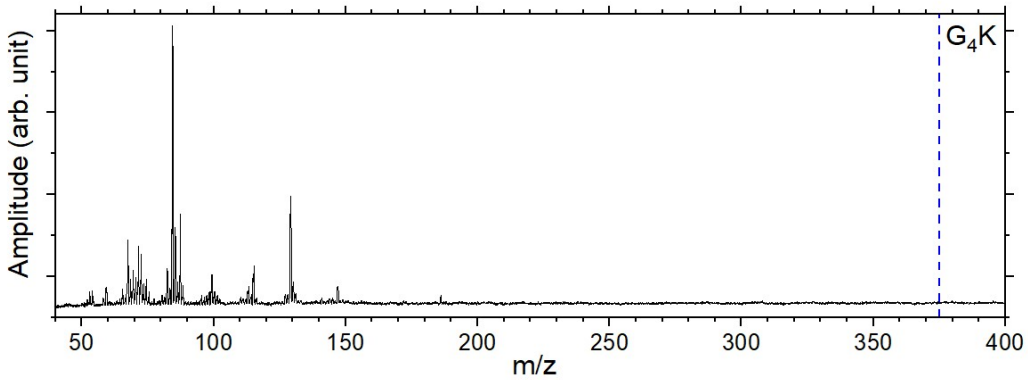

Figure S6: Photodissociation mass spectrum over the full mass range of G_4K measured at 401.6 eV (BESSY II). Here, the mass window was set to see the fragment from m/z 50 to m/z 160. The dashed blue line represents the position of the precursor ion.

Mass	G_5/G_3	PG_4	G_4H	G_4R	G_4K
28	$C_2H_4^+$/ CH_2N^+				
29	CHO^+				
30	G				
31	CH_3O^+				
42	$C_2H_4N^+$				
43	$CHNO^+$				
45	$COOH^+$				
55	C_2NOH^+	C_2NOH^+			
56	$C_2NOH_2^+$	$C_2NOH_2^+$			
67					$C_5H_7^+$
68		$[P-2H]^+$			
70		P		$C_4H_8N^+$	
71		$[P+H]^+$		$C_4H_7O^+$	
72				$C_4H_{10}N^+$	
81			$C_4H_5N_2^+$		
82			$C_4H_6N_2^+$		
83			$C_4H_7N_2^+$		
84					$C_5H_{10}N^+$
85				$C_3H_3NO_2^+$	
87			a_2	$C_4H_9NO^+/a_2$	a_2
88				$C_4H_{10}NO^+$	
93			$C_5H_5N_2^+$		
110			$C_5H_8N_3^+$		
112				$C_5H_{10}N_3^+$	
115			GG/b_2	GG/b_2	GG/b_2
131					y_1-NH_3
147					y_1

Table S1: Attribution of the fragments observed during our study for each peptide.

Experimental nitrogen K-edge partial ion yield spectra

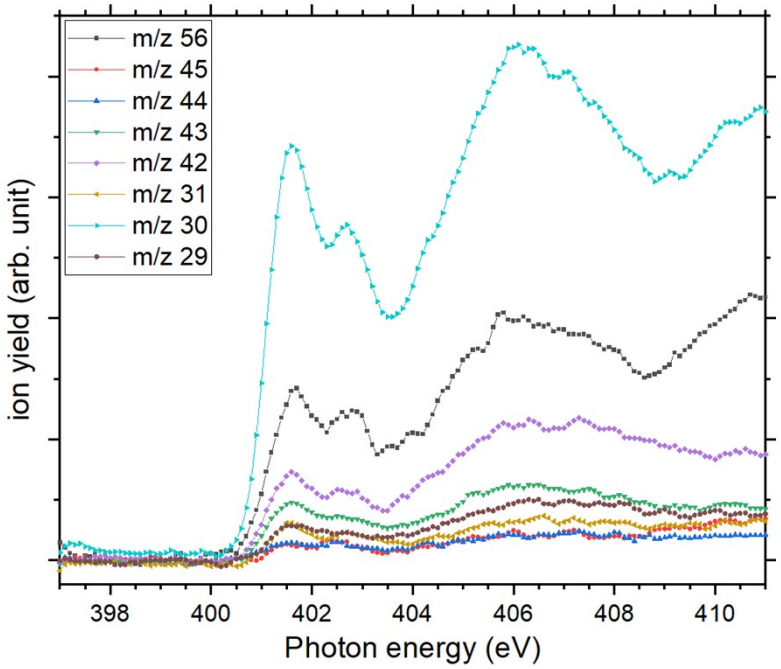

Figure S7: Experimental nitrogen K-edge partial ion yield spectra of G_5.

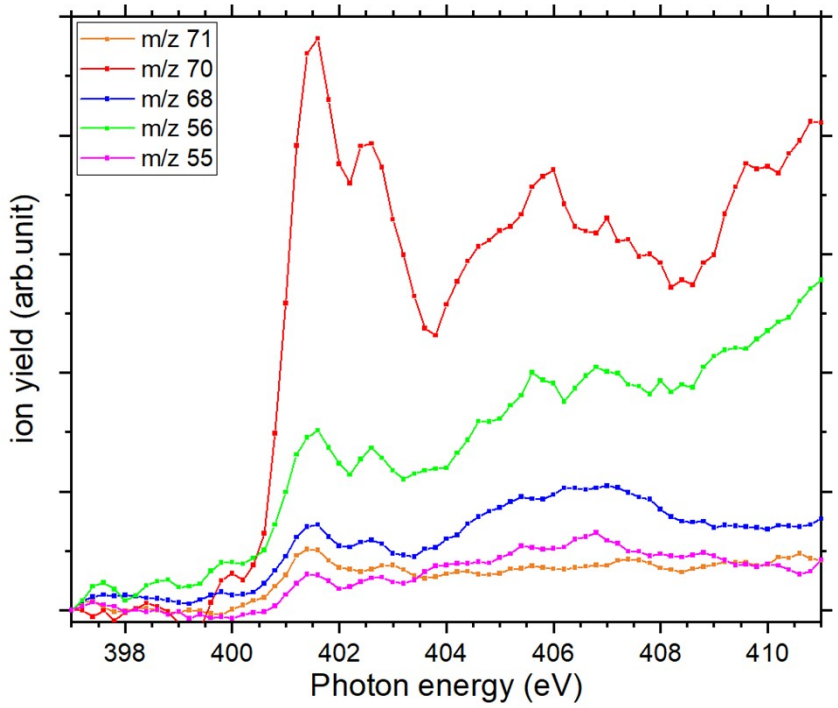

Figure S8: Experimental nitrogen K-edge partial ion yield spectra of PG_4.

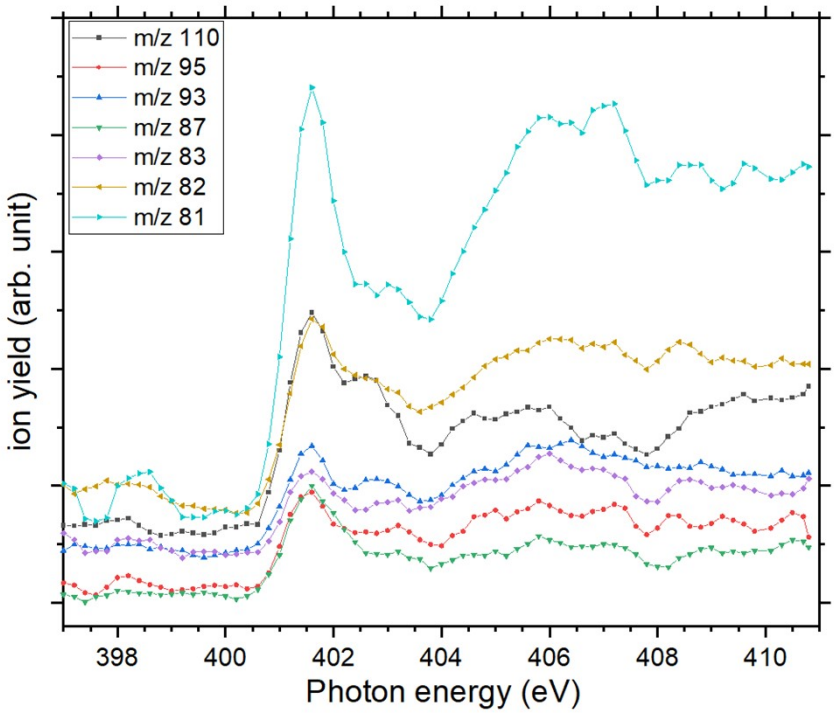

Figure S9: Experimental nitrogen K-edge partial ion yield spectra of G_4H.

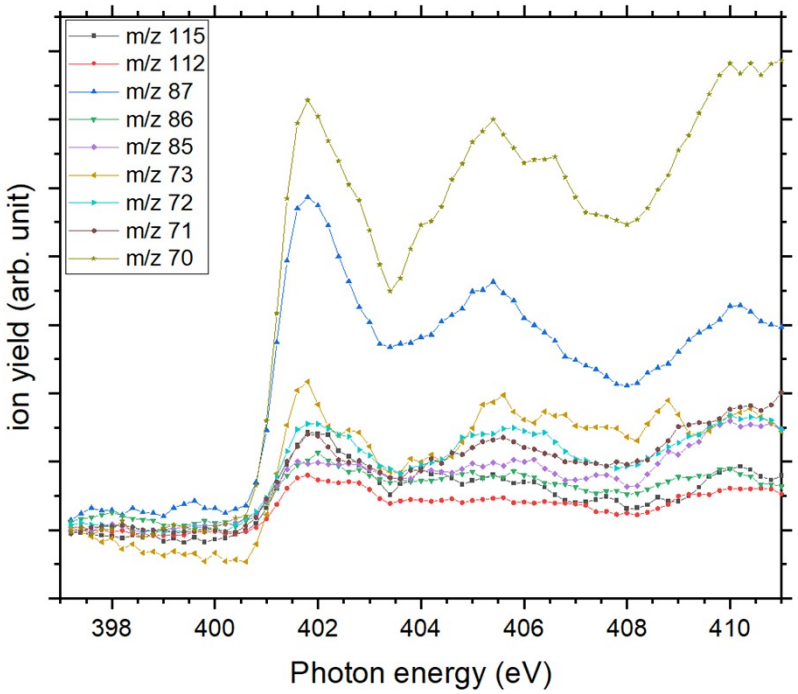

Figure S10: Experimental nitrogen K-edge partial ion yield spectra of G_4R.

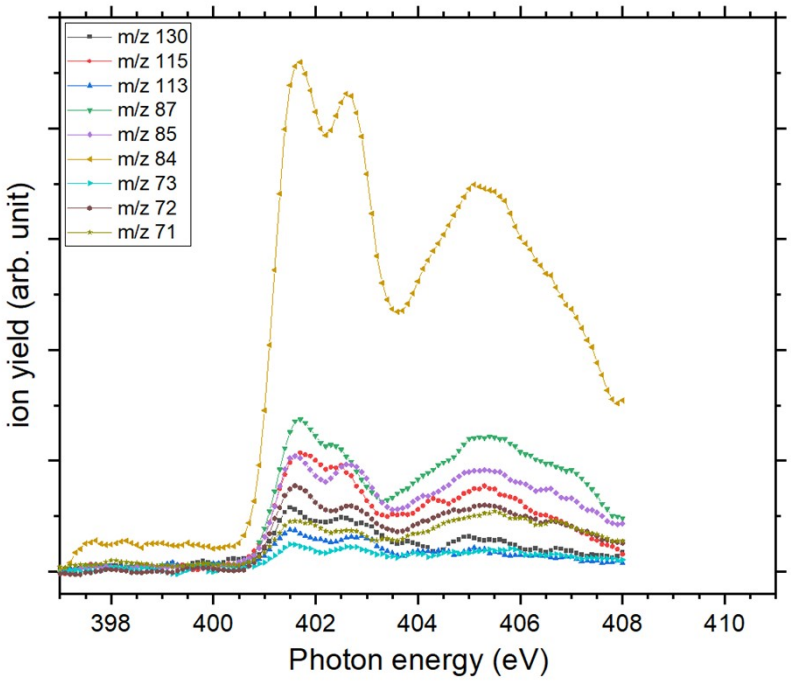

Figure S11: Experimental nitrogen K-edge partial ion yield spectra of G_4K.

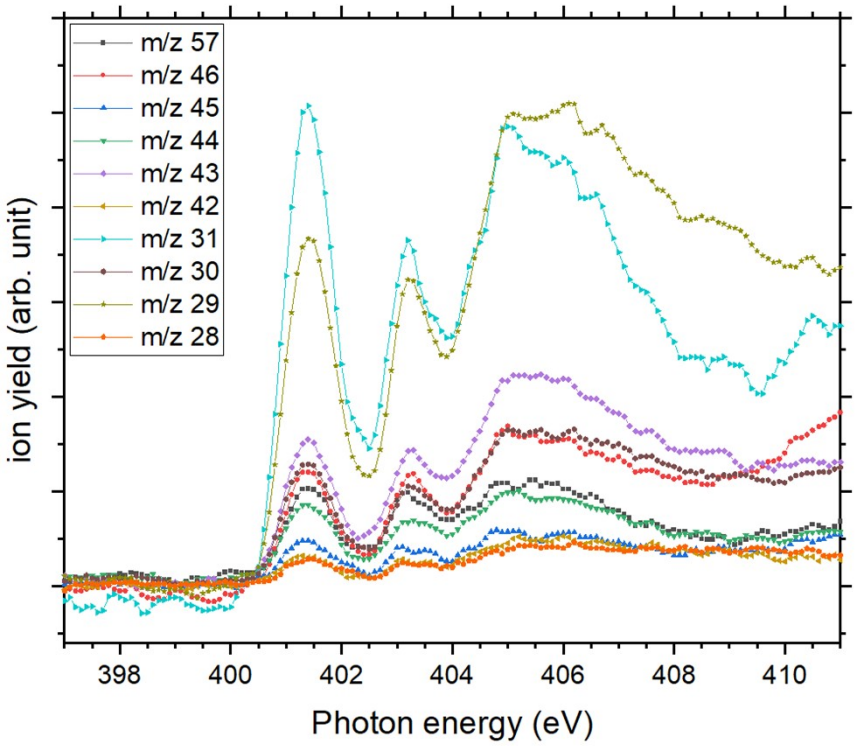

Figure S12: Experimental nitrogen K-edge partial ion yield spectra of G_3.

Molecular orbitals and structures

G5

Conformer 1

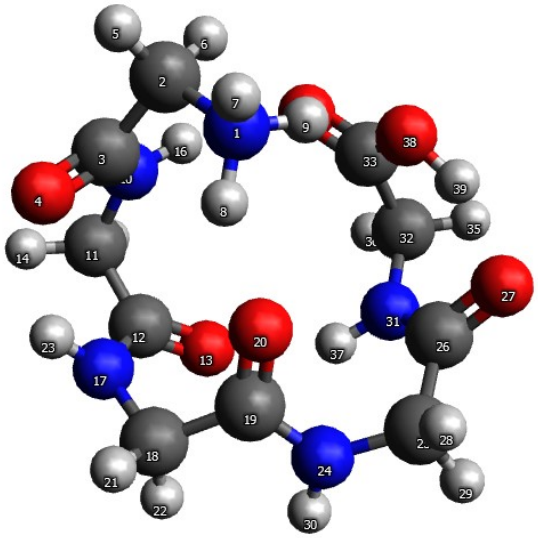

Figure S13: DFT-optimized geometry of conformer 1 of G_5 (B3LYP/ZORA-TZVP).

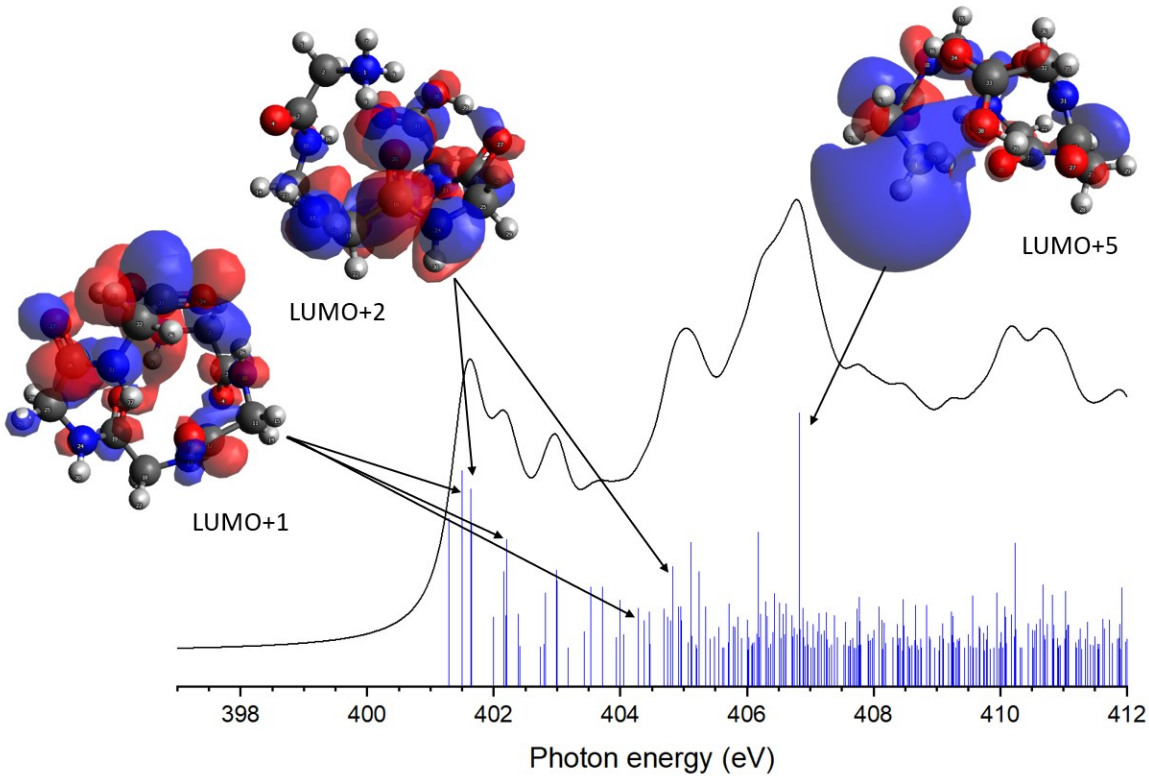

Figure S14: Calculated spectrum of conformer 1 of G_5 with the respective LUMOs responsible for the main transitions.

Conformer 2

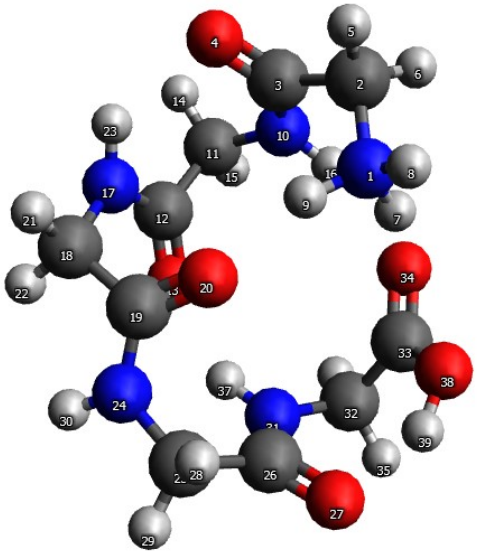

Figure S15: DFT-optimized geometry of conformer 2 of G_5 (B3LYP/ZORA-TZVP).

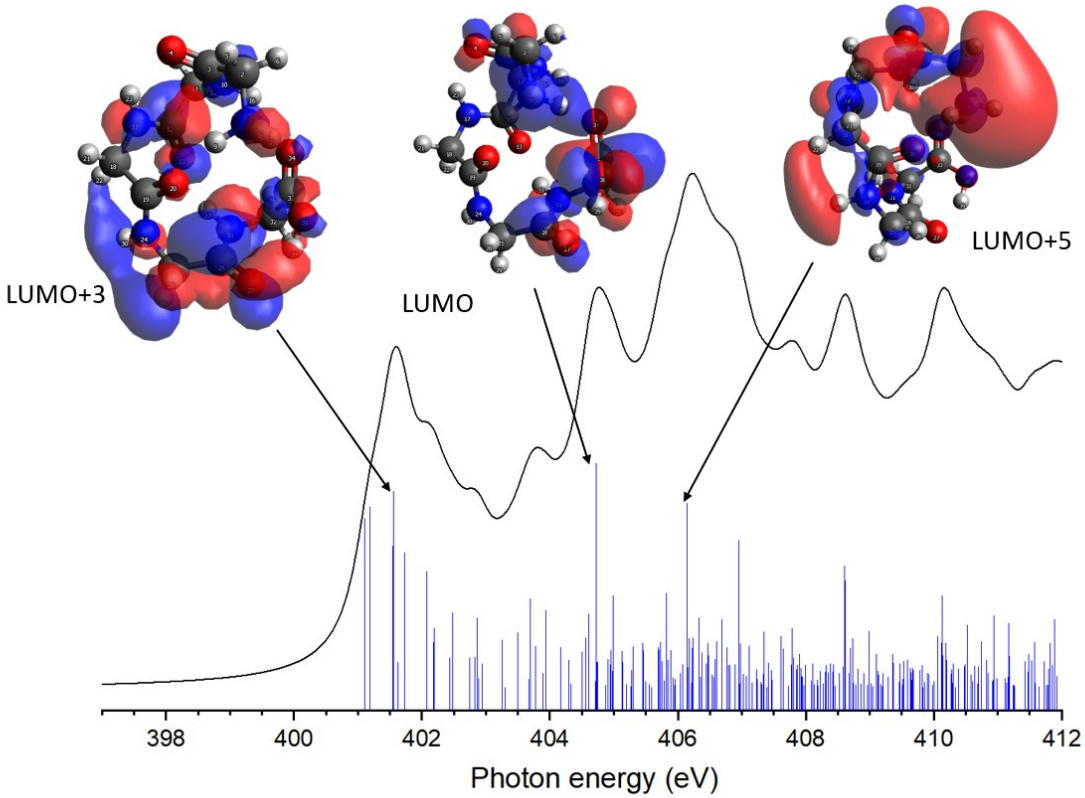

Figure S16: Calculated spectrum of conformer 2 of G_5 with the respective LUMOs responsible for the main transitions.

PG_4

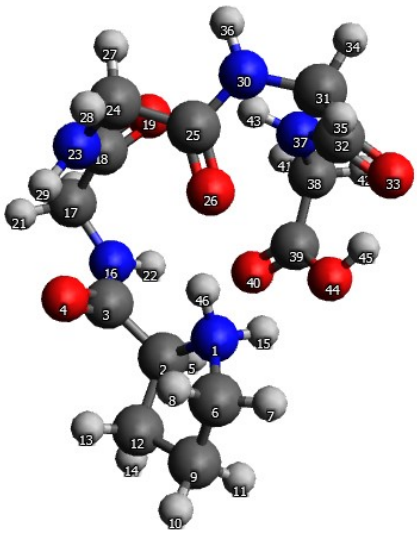

Figure S17: DFT-optimized geometry of PG_4 (B3LYP/ZORA-TZVP).

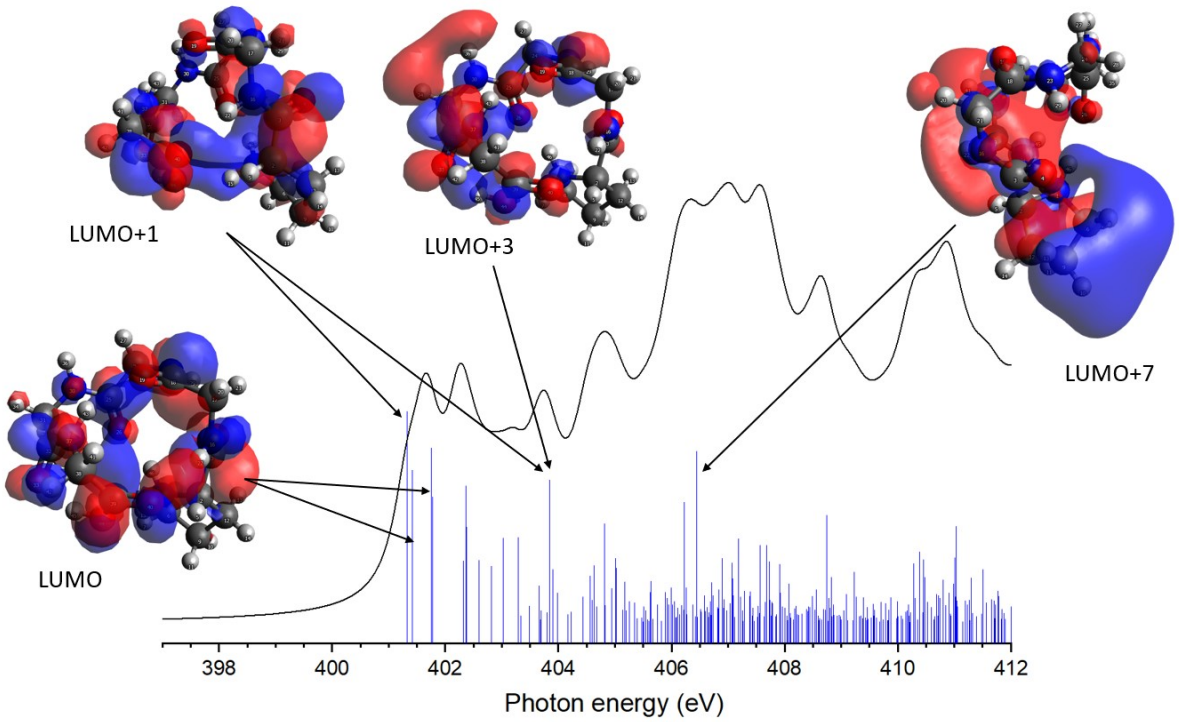

Figure S18: Calculated spectrum of PG_4 with the respective LUMOs responsible for the main transitions.

G_4H

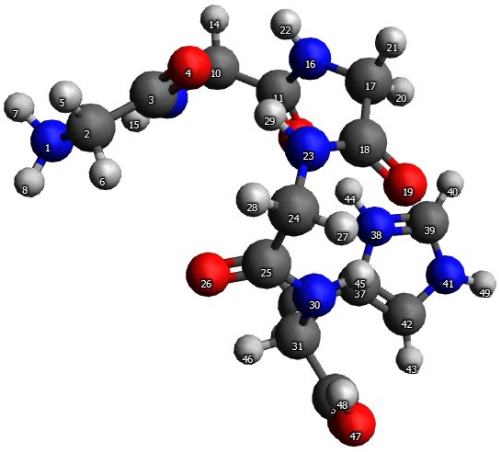

Figure S19: DFT-optimized geometry of G_4H (B3LYP/ZORA-TZVP).

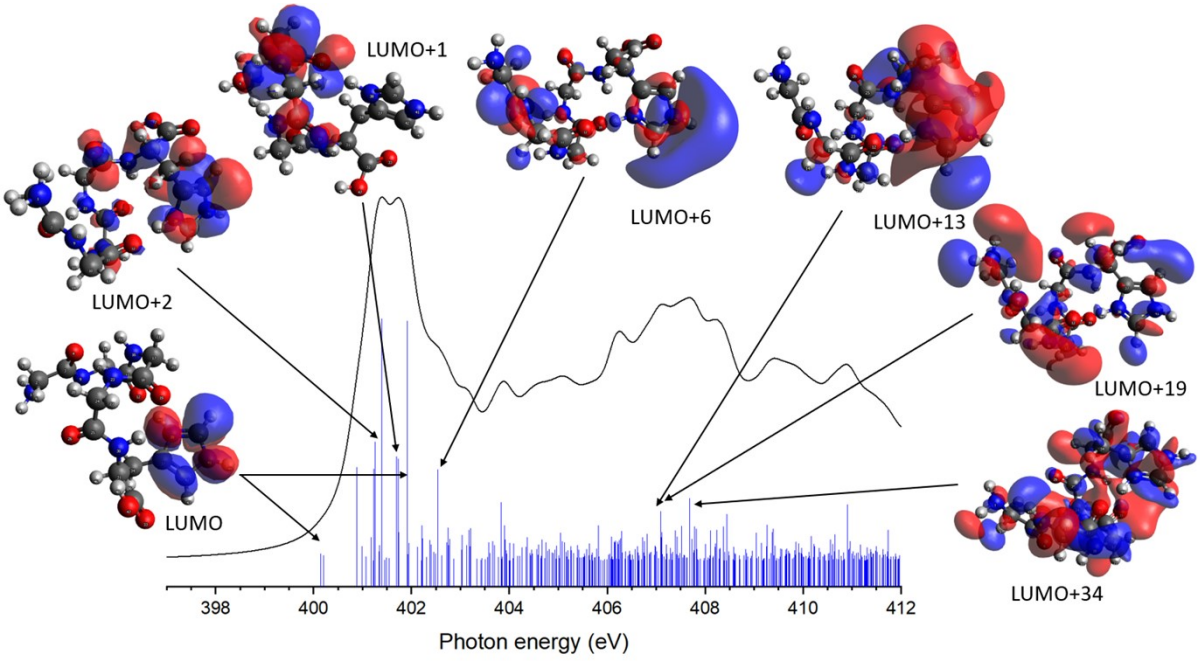

Figure S20: Calculated spectrum of G_4H with the respective LUMOs responsible for the main transitions.

G_4R

Conformer 1

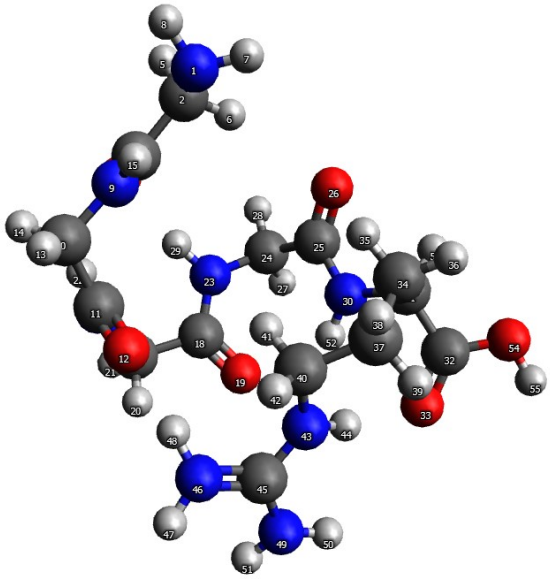

Figure S21: DFT-optimized geometry of conformer 1 of G_4R (B3LYP/ZORA-TZVP).

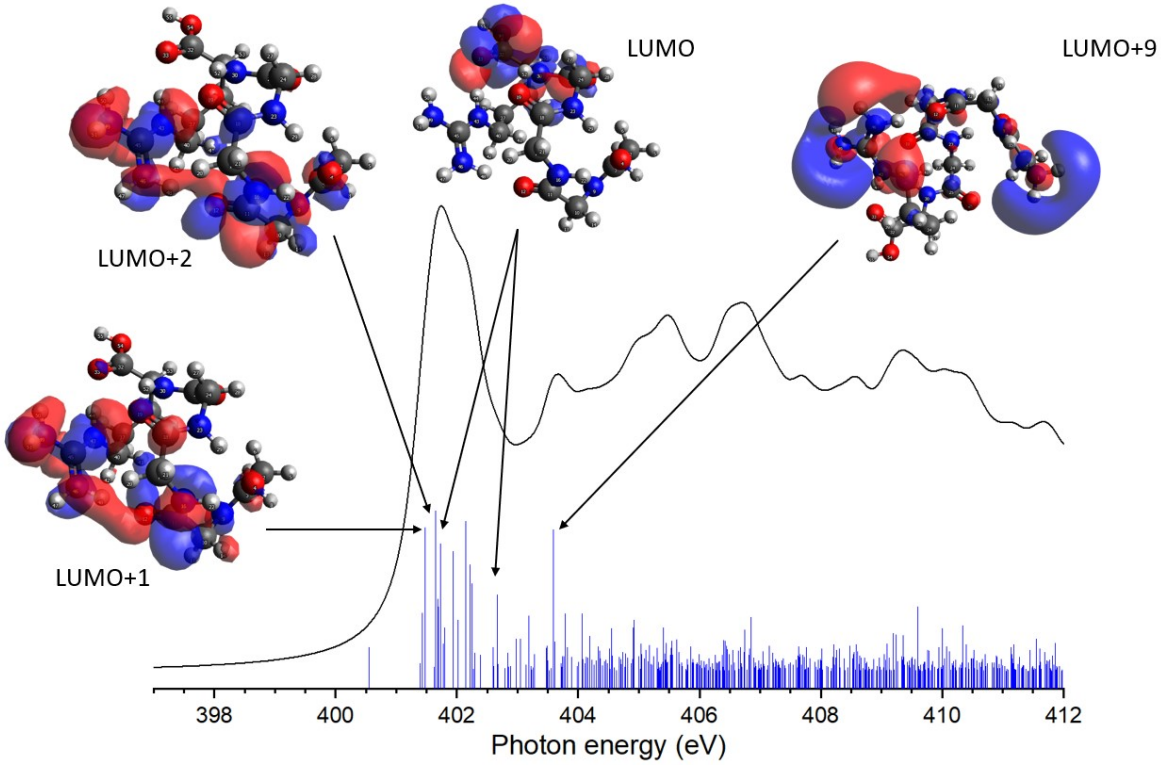

Figure S22: Calculated spectrum of conformer 1 of G_4R with the respective LUMOs responsible for the main transitions.

Conformer 2

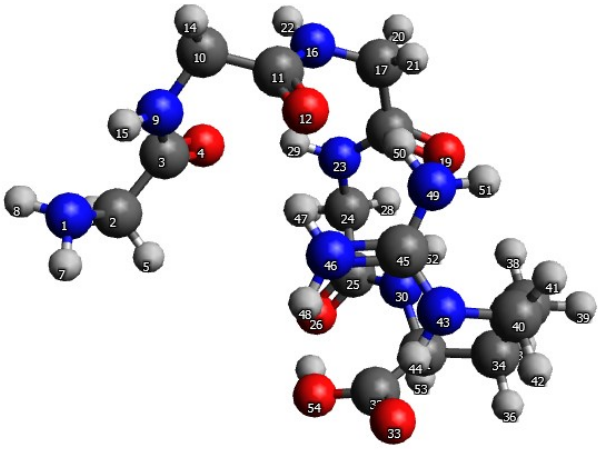

Figure S23: DFT-optimized geometry of conformer 2 of G_4R (B3LYP/ZORA-TZVP).

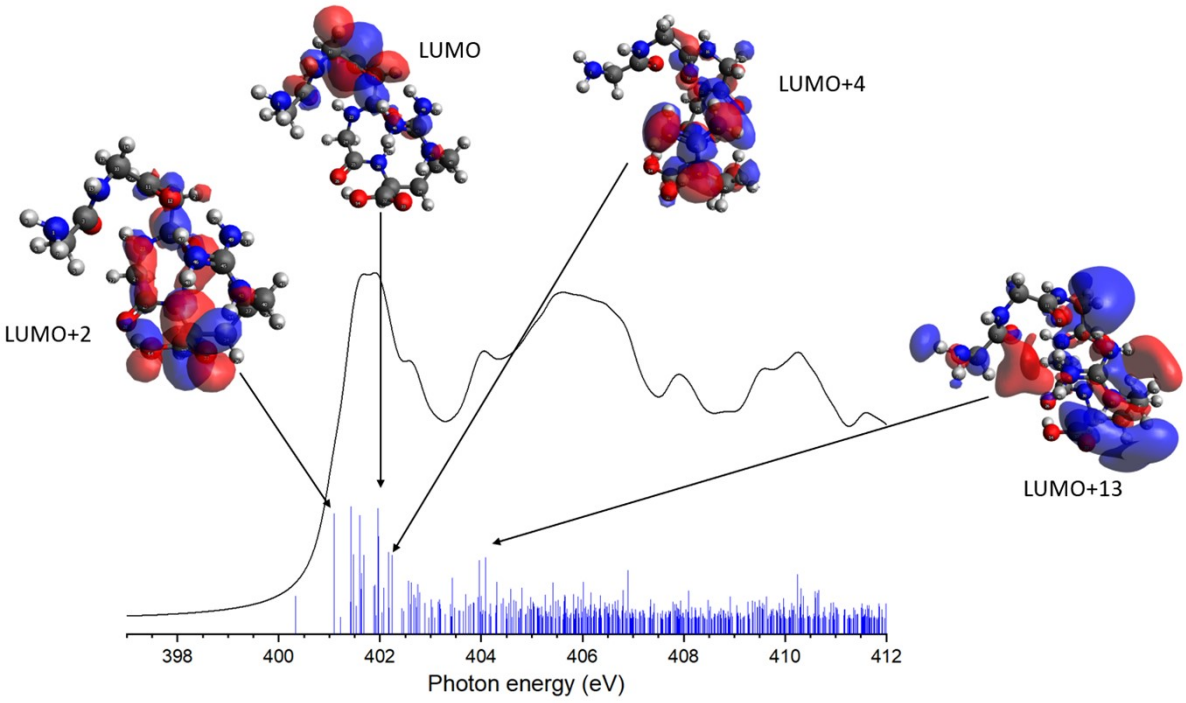

Figure S24: Calculated spectrum of conformer 2 of G_4R with the respective LUMOs responsible for the main transitions.

G_4K

Conformer 1

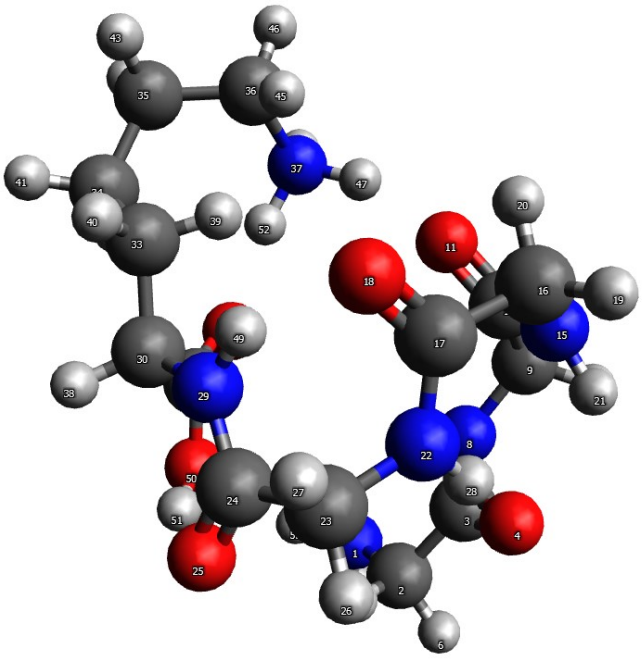

Figure S25: DFT-optimized geometry of conformer 1 G_4K (B3LYP/ZORA-TZVP).

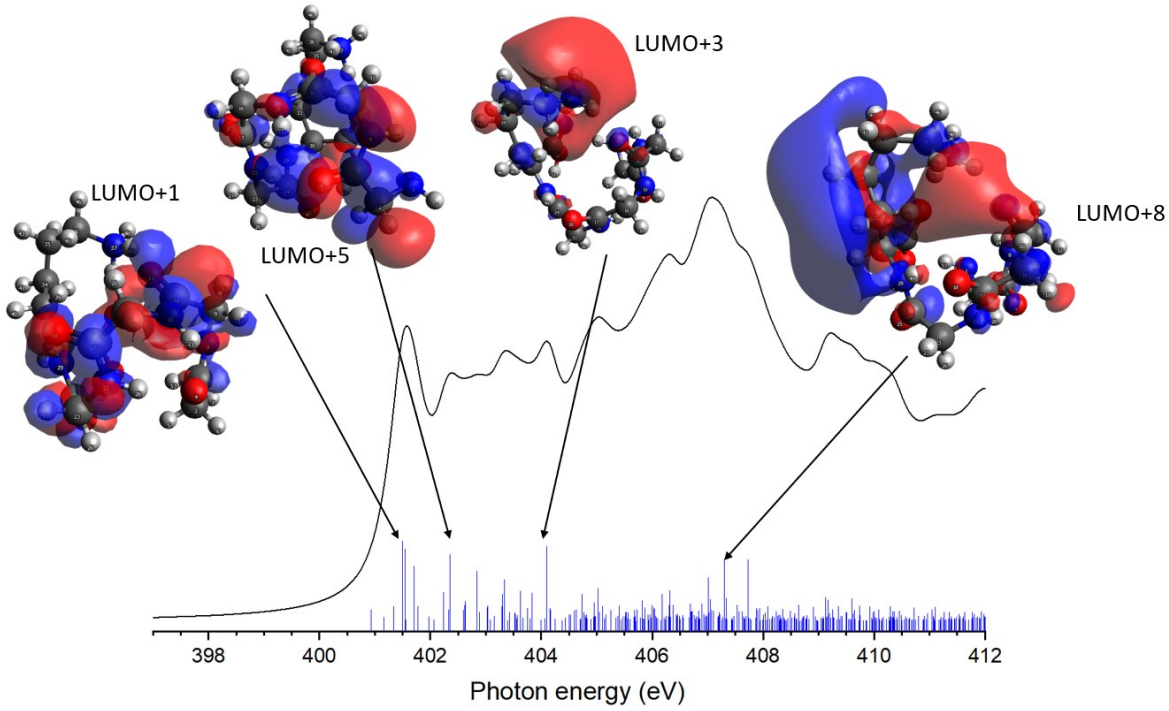

Figure S26: Calculated spectrum of conformer 1 of G_4K with the respective LUMOs responsible for the main transitions.

Conformer 2

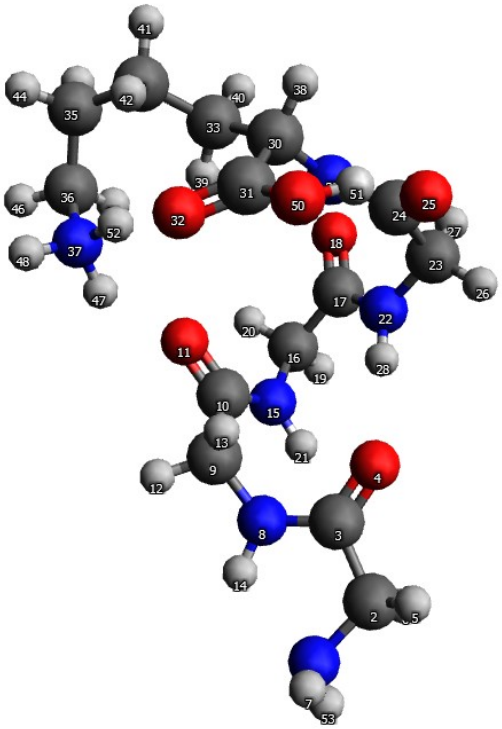

Figure S27: DFT-optimized geometry of conformer 2 G_4K (B3LYP/ZORA-TZVP).

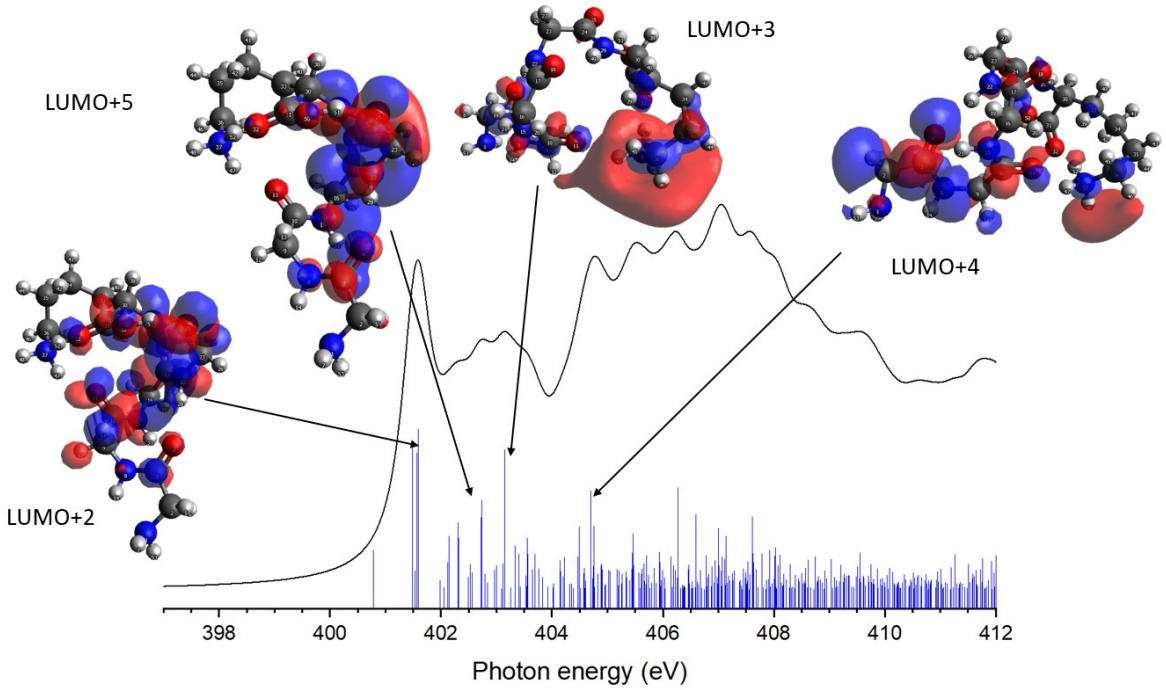

Figure S28: Calculated spectrum of conformer 2 of G_4K with the respective LUMOs responsible for the main transitions.

GGG

GGGH1

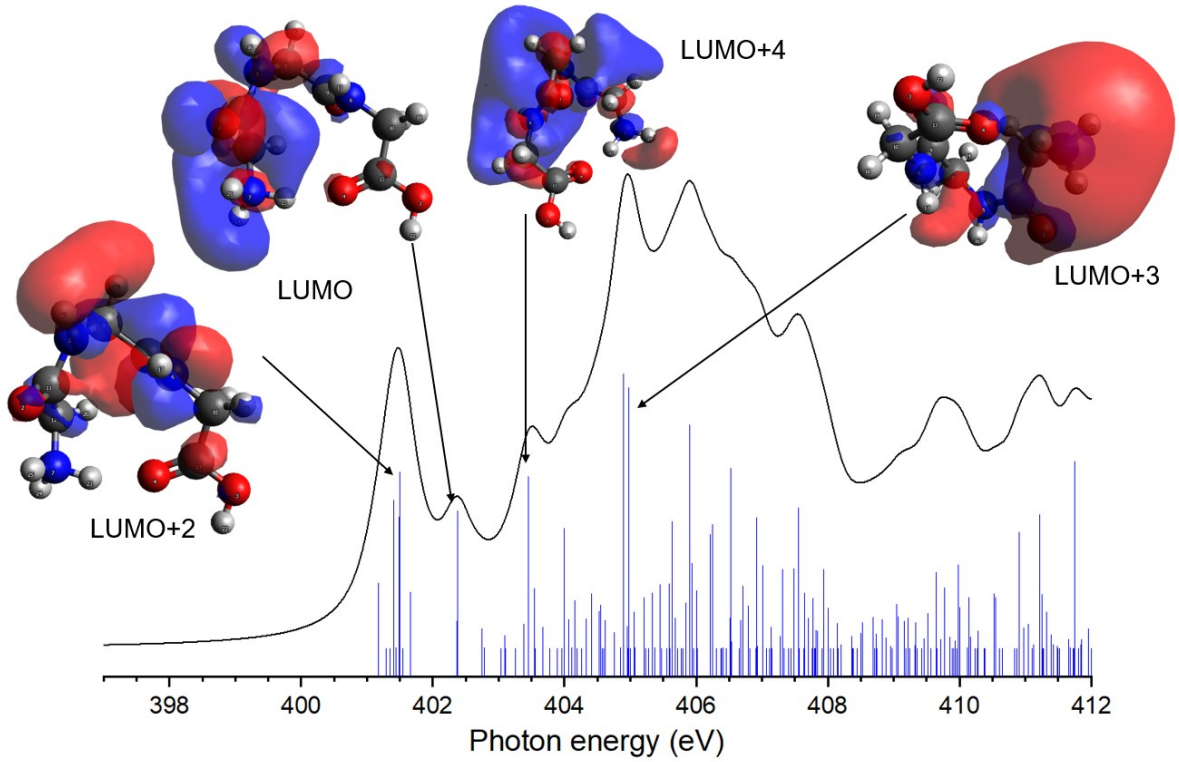

Figure S29: Calculated spectrum of GGGH1 at the N K-edge with the respective LUMOs responsible for the main transitions.

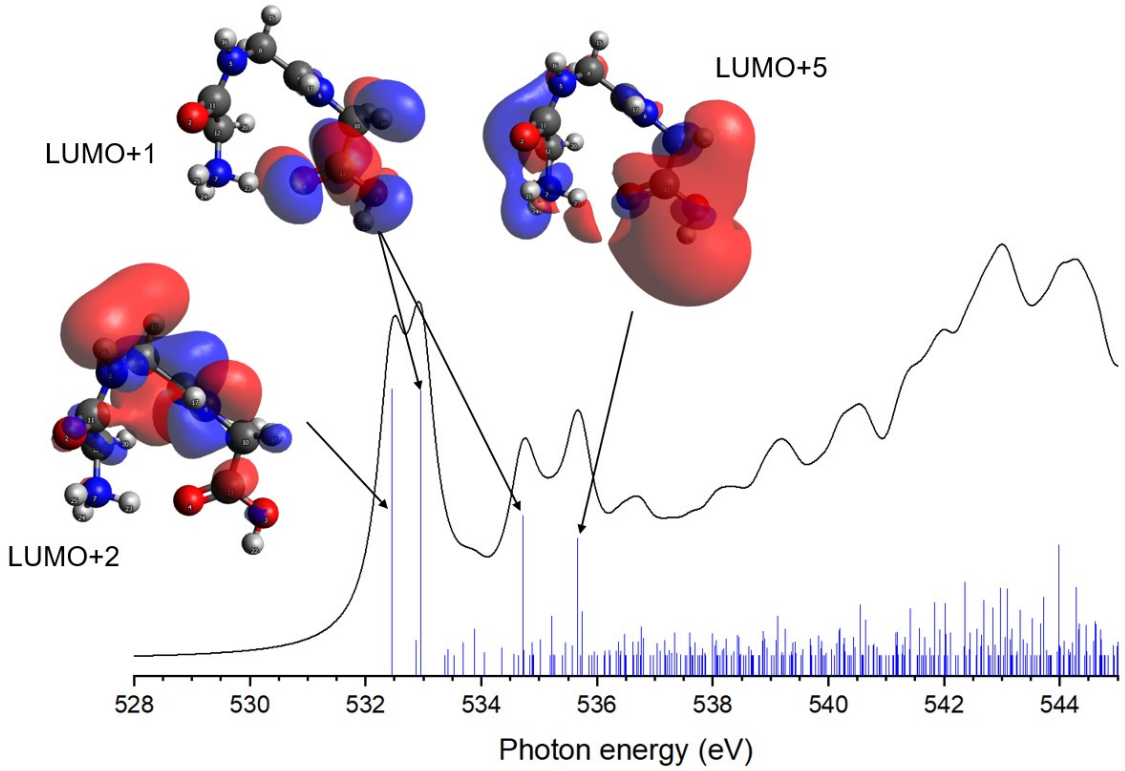

Figure S30: Calculated spectrum of GGGH1 at the O K-edge with the respective LUMOs responsible for the main transitions.

GGGH2

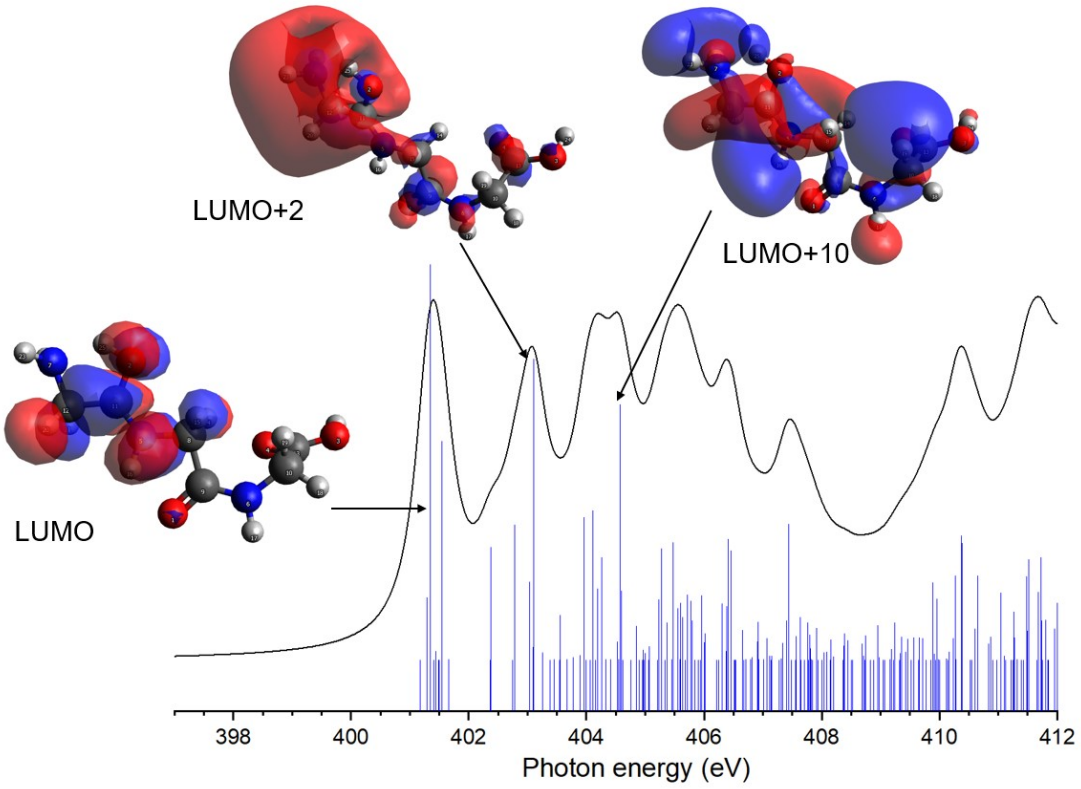

Figure S31: Calculated spectrum of GGGH2 at the N K-edge with the respective LUMOs responsible for the main transitions.

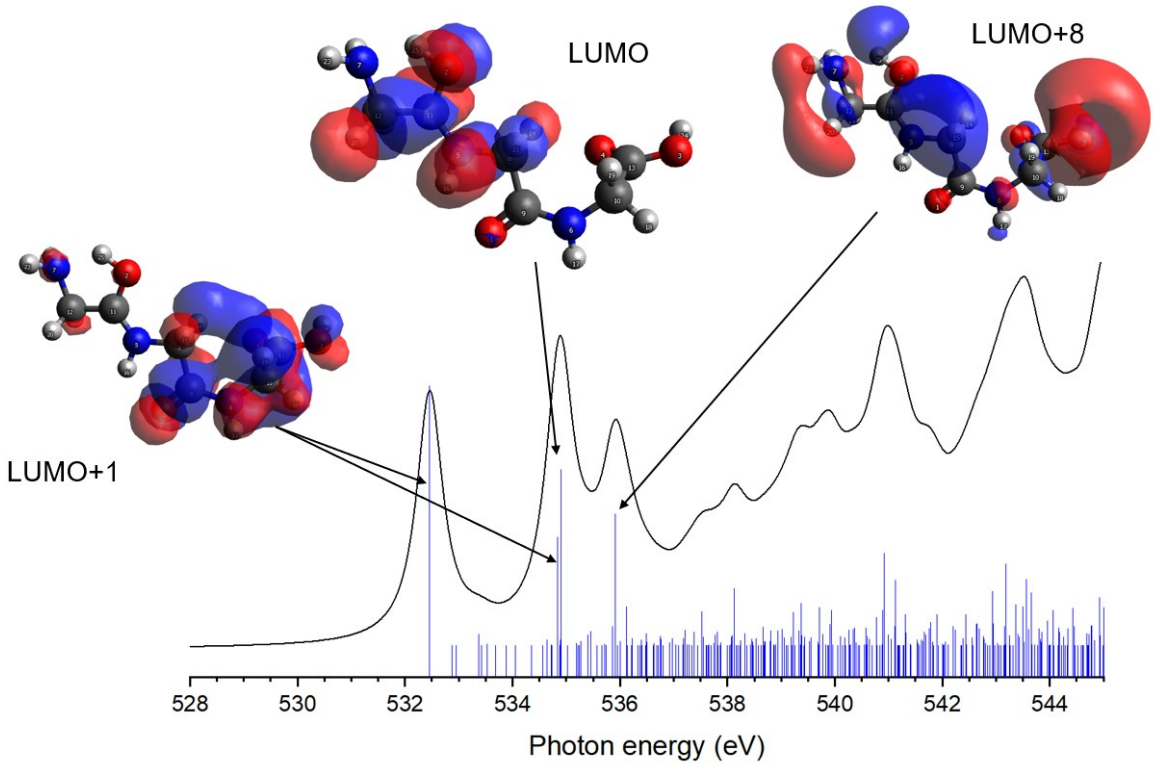

Figure S32: Calculated spectrum of GGGH2 at the O K-edge with the respective LUMOs responsible for the main transitions.

NEXAMS spectra of G_5 and G_3 at the C K-edge

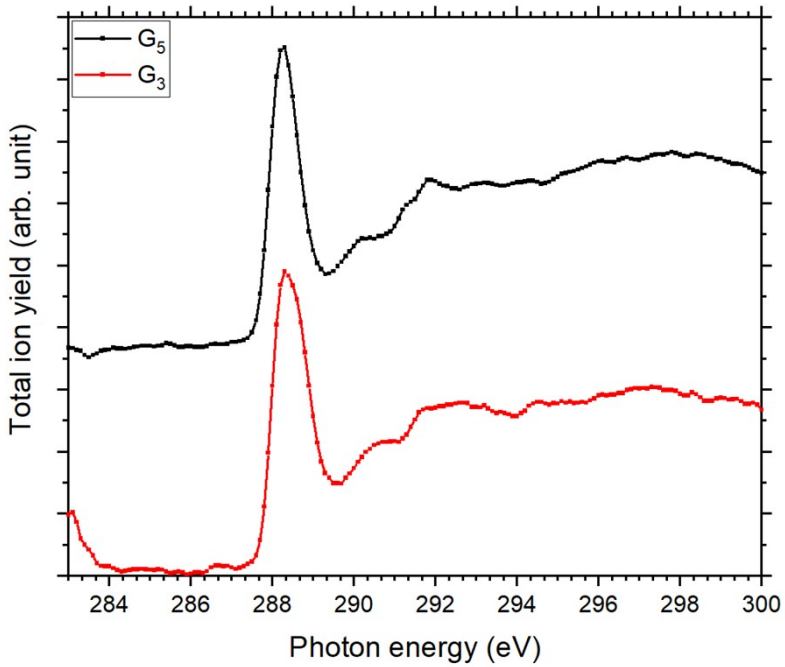

Figure S33: Experimental carbon K-edge total ion yield spectra of G_5 in black, and in red G_3.

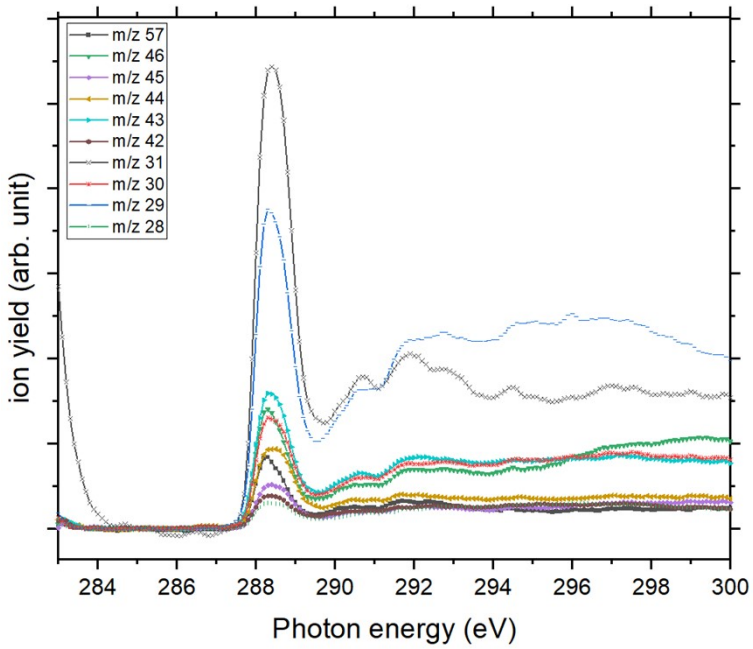

Figure S34: Experimental carbon K-edge partial ion yield spectra for G_3.

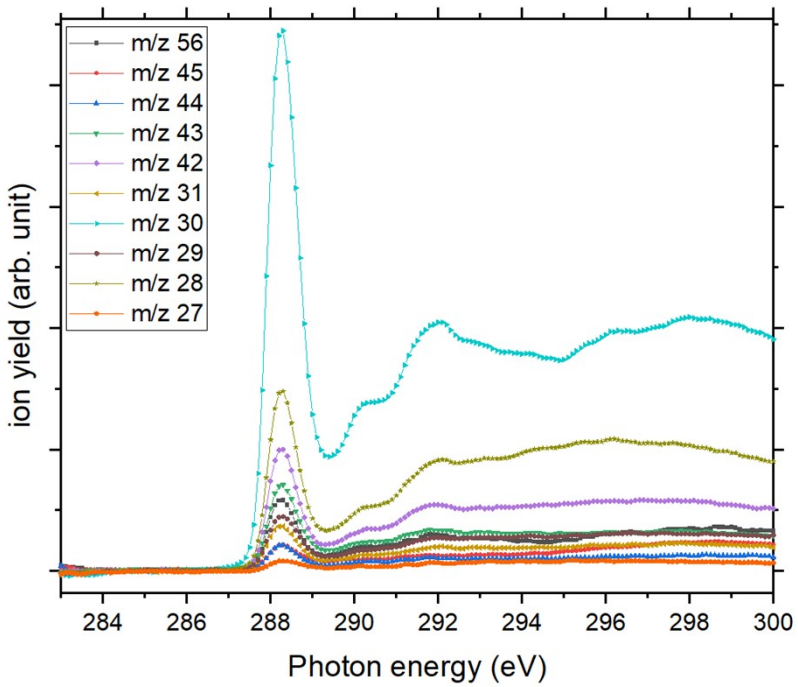

Figure S35: Experimental carbon K-edge partial ion yield spectra for G_5.

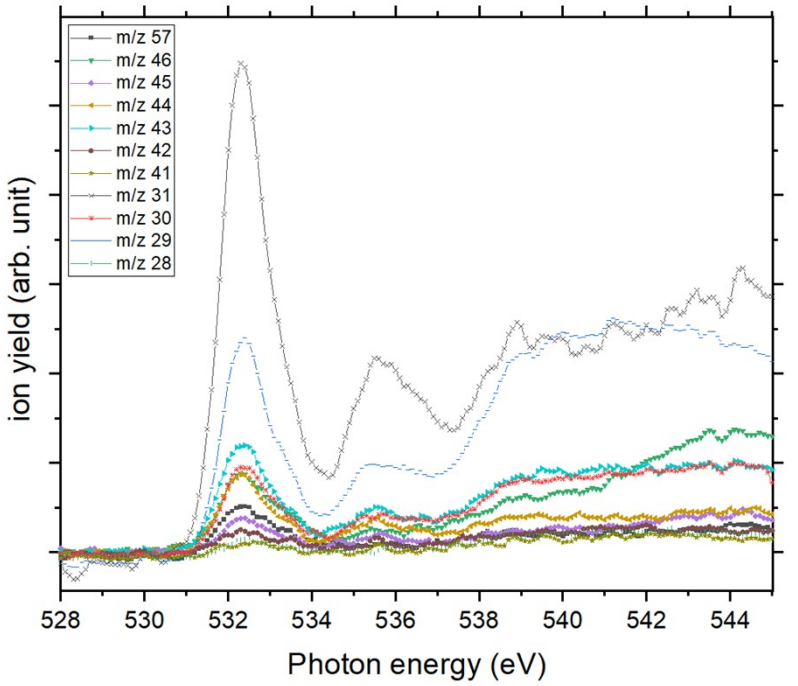

Figure S36: Experimental oxygen K-edge partial ion yield spectra of G_3.

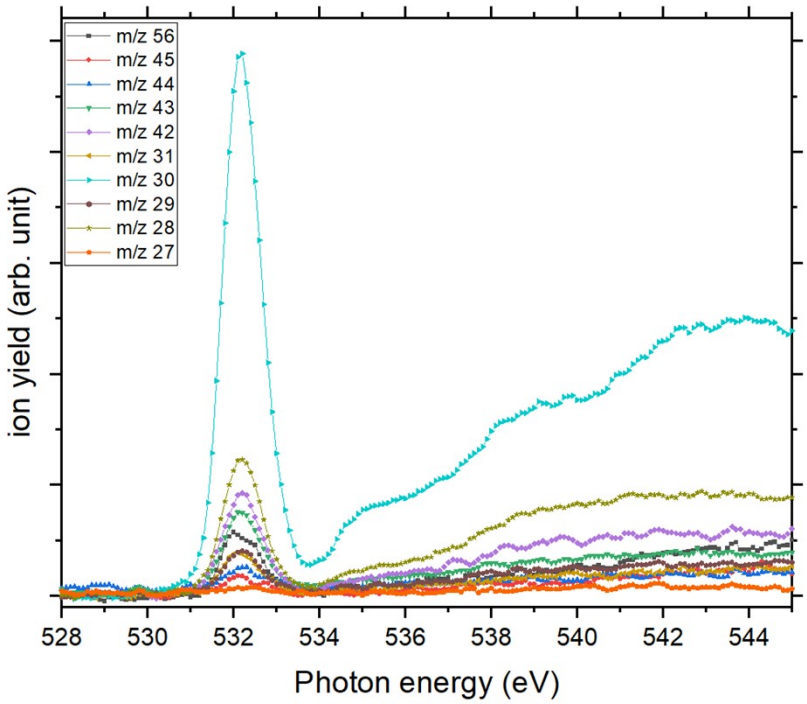

Figure S37: Experimental oxygen K-edge partial ion yield spectra of G_5.